FACILITY FOR ANTIPROTON AND ION RESEARCH

# Technical Report
# for the Design, Construction and Commissioning of the *SiM-X Project: Silicon Microcalorimeters for high-precision X-ray spectroscopy*


S. Kraft-Bermuth and P. Egelhof
on behalf of the SiM-X Collaboration

**Abstract**

The precise determination of electron transition energies in highly-charged ions by means of X-ray spectroscopy is one important focus of research within APPA/SPARC. One novel approach for high-resolution X-ray detection is the use of so-called "microcalorimeters", which detect the energy of an incoming X-ray as heat rather than by charge production and, therefore, combine a large dynamic range with excellent energy resolution. This novel detector concept has already proven its feasibility as a high-resolution X-ray spectrometer in several ESR experiments and an excellent energy resolution of $\Delta E/E \sim 10^{-3}$ has been demonstrated for X-ray energies of 50–100 keV. However, for the application at FAIR, the existing detector technology needs to be further improved, in particular with respect to detector solid angle.

In this Technical Design Report, the preparation of large arrays of silicon microcalorimeters for high-resolution X-ray spectroscopy (SiM-X) is presented. The detector that has been used in the ESR experiments has an active detector area of 10 mm², which results in an overall detection efficiency of about $10^{-6}$ at the current ESR gas-jet target. For future experiments this active area will be increased to about 90 mm² by increasing the number of single detector pixels. To achieve this purpose, a more compact cryogenic setup will be designed and tested. Hereby, we pursue a staged approach, starting with a detector array with an active area of about 30 mm² and then increasing the active area by deploying three arrays in total.

For the experiments at ESR, CRYRING and HESR, the focus lies on the detection of high-energy X-rays with energies of 50–100 keV. However, at the HITRAP facility, also low-energy X-rays with energies less than 10 keV will be investigated. Therefore, two different microcalorimeter arrays, one optimized for high X-ray energies around 100 keV, and one for X-ray energies below 20 keV, will be prepared in parallel. The experimental setup will be very similar for both detectors, only the size of the X-ray absorbers has to be adjusted. The time schedule foresees to have the detector functional and tested when the Modularized Start Version of FAIR starts to operate in 2018. Among the first experiments that can be performed at ESR and CRYRING will be experiments to investigate the 1s Lamb Shift in hydrogen-like atoms and experiments on Lithium- or Beryllium-like ions which will investigate configuration interactions in few-electron-systems.

## Members of the *SiM-X* Collaboration:

Germany

Institute for Atomic and Molecular Physics, Justus-Liebig-University, Gießen:
Saskia Kraft-Bermuth, Artur Echler, Pascal Scholz

GSI-Helmholtz Center for Heavy Ion Research, Darmstadt:
Peter Egelhof, Alexander Bleile, Patrick Grabitz

Russia

Lomonosov Moscow State University, Moscow:
Victor Andrianov

USA

Department of Physics, University of Wisconsin, Madison:
Dan McCammon

Contents

## 1. Introduction and overview

Within the SPARC (Stored Particles Atomic Research Collaboration) program, high-resolution X-ray spectroscopy is one important focus of research. The aim is to precisely determine the transition energies of electrons in various ions and charge states and to compare them with quantum electrodynamics calculations. The new accelerator facility FAIR will offer a unique experimental infrastructure for these investigations: A multi storage-ring complex, consisting of the already operational ESR in combination with the newly installed CRYRING as well as the high-energy storage ring HESR, will provide a wide selection of stable as well as unstable nuclides in beams of unparalleled intensity in a wide range of energies from 760 MeV/u down to 0.5 MeV/u. In addition, in the ion trap facility HITRAP ions will be decelerated to rest, thus providing a point-like X-ray source, free of Doppler corrections which present a major source of systematic uncertainties in such experiments. To fully exploit the experimental opportunities, high-resolution X-ray spectrometers are required. Due to the expected count rates, such detectors need not only to have an excellent energy resolution and a large dynamic range, but also a reasonable detection efficiency and solid angle in order to allow for the spectroscopy of rare species.

For the wide variety of experiments foreseen within the SPARC program, several different detector concepts are developed. One concept is the concept of so-called "microcalorimeters". As compared to conventional germanium detectors, this concept improves the X-ray energy resolution by at least one order of magnitude. In comparison to crystal spectrometers, which obtain a similar energy resolution, microcalorimeters offer the advantage of a large dynamic range and – due to the possibility of using detector arrays – relatively large solid angle coverage and high overall detection efficiency. Their development and optimization is, therefore, an integral part of the SPARC technical proposal [1].

Due to the unique availability of bare and highly-charged ions of highest nuclear charge at FAIR, the focus of the present technical design report lies on the development of silicon microcalorimeters for hard X-rays in the energy range of 50–100 keV. In this energy range, atomic physics experiments focus on the investigation of fundamental interactions in highest Coulomb fields. Some examples are listed below:

- The precise determination of the 1s Lamb Shift in hydrogen-like ions provides a most sensitive test of quantum electrodynamics in highest Coulomb fields ($Z\alpha \approx 1$), not accessible otherwise [2,3]. At present, the experiments reach an accuracy of around ±5 eV. However, to scrutinize theoretical calculations, an accuracy of ±1 eV or better is mandatory.
- Once the Lamb Shift has been determined in stable isotopes with sufficient accuracy, the influence of the nuclear charge radius on the Lamb Shift can be used to determine nuclear charge radii, which will be of particular interest for exotic, rare or unstable nuclei.
- The precise determination of the classical Lamb Shift in the $2s_{1/2}$-$2p_{1/2}$ transition is a special challenge for highly-charged ions, because the transition energy of the order of 50–100 eV is difficult to access with the standard method of laser spectroscopy.
- Inner-shell transitions in helium-, lithium- or beryllium-like heavy ions provide a test of few-electron-systems which have become accessible for highly accurate calculations only recently. In these systems, not only transition energies but also transition probabilities are of great interest, in particular for the decay properties of the singly excited $1s2s^2$ state in Lithium-like very heavy ions. The particular feature of this state is the occurrence of an exotic, dipole allowed, "Two-Electron One-Photon" (TEOP) decay into the $1s^2 2p_{1/2}$ and the $1s^2 2p_{3/2}$ levels, mediated by configuration interaction [4,5].

These investigations at high X-ray energies will be complemented by investigations in the X-ray energy regime of 1–10 keV. For example, the investigation of the Balmer transitions in highly-charged ions offers not only a verification of calculations of capture cross sections [6], but can also help to minimize experimental uncertainties in the Lamb Shift experiments. Moreover, this low-energy regime is of interest for the investigation of outer-shell transitions in lithium-like high-Z ions. It will, therefore, be of particular interest to investigate such ions with broad-band X-ray detectors in both energy regimes.

Silicon microcalorimeters for the spectroscopy of hard X-rays at storage rings have been proposed, developed and applied at GSI by Egelhof et al. since more than two decades [7-9]. The detection principle and layout will be discussed in detail in section 2.2. Here it shall only be mentioned that these microcalorimeters can be easily adjusted to the desired range of X-ray energies by simply varying the heat capacity, i.e. the material and the thickness of the X-ray absorber. For X-ray energies of 50–100 keV, the current detector setup obtains a relative energy resolution of $\Delta E/E \sim 10^{-3}$. With an active detector area of 10 mm², it provides an overall detection efficiency of $1 \times 10^{-6}$, which is already about one order of magnitude larger than the detection efficiency of a crystal spectrometer with comparable energy resolution [10]. Metallic magnetic calorimeters (MMCs), which are currently investigated by the group of C. Enss et al. in Heidelberg [11], have also been demonstrated to obtain excellent energy resolution and good overall detection efficiency and are certainly a promising concept. However, the active area is currently reported to be about 8 mm² [12], and to our knowledge the parallel readout of many detectors has not yet been demonstrated. Although it is stated that the MMCs obtain high detection efficiency per pixel because they use absorbers of gold, a large solid angle remains an essential requirement.
The combination of two different microcalorimeter setups with comparable energy resolution and detection efficiency will minimize systematic effects. It will also allow performing angular spectroscopy, thereby investigating nuclear properties.

The aim of this technical design report is to develop the next generation of silicon microcalorimeters for the application at FAIR. Especially when the investigation of rare or short-lived nuclei is intended, a further increase in detection solid angle is needed. Therefore, we propose to extend the currently available detector setup to obtain an active area of about 90 mm², which will be realized mainly by increasing the number of available single detector pixels. In parallel, we will further improve the energy resolution by optimizing readout electronics, data acquisition and experimental setup. As can be deduced from the proposed time schedule, we expect to have an array of silicon microcalorimeters with an active area of about 90 mm² fully tested when the first ion beams will be available as expected in 2018. As ESR and CRYRING will be among the first facilities of FAIR that will be fully operational, Lamb Shift experiments on a variety of nuclides can start immediately. It will be of particular interest to repeat the investigation of the Lamb Shift in hydrogen-like uranium, which has been conducted with great success already at the ESR [13], at CRYRING using silicon microcalorimeters to improve the accuracy of the ESR investigations. The first high-resolution investigation of the above-mentioned TEOP can also be addressed

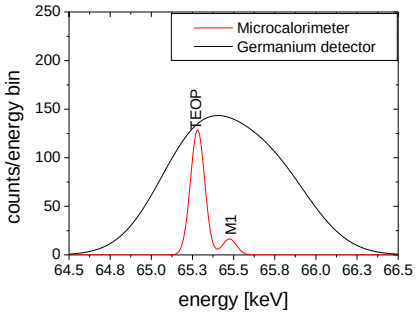


**Figure 1:** Example for the performance of a microcalorimeter as compared to a germanium detector. Shown is a simulation of the spectrum of beryllium-like uranium with the TEOP transition.

immediately. Figure 1 shows a simulated example spectrum and compares a high-resolution germanium detector with the performance of a microcalorimeter. For these measurements, it will be interesting to exploit the intrinsic Doppler correction by using the Doppler-shifted Balmer lines as reference. This will also serve as a benchmark test for HESR experiments. Furthermore, the determination of line widths will provide information on the properties of targets and ion beams at the new facility.

## 2. Physics requirements

### 2.1. X-ray spectroscopy at the FAIR storage rings

Experiments to determine the Lamb shift in hydrogen-like ions as well as investigations of helium- or lithium-like ions will be performed at the Experimental Storage Ring (ESR) in combination with CRYRING or at the High-Energy Storage Ring HESR. The experimental procedure is similar: A beam of highly-charged ions is injected into the storage ring, cooled and in certain cases decelerated. Then the ions pass through either the gas-jet of an internal gas-jet target or through an electron target. The development of improved gas-jet targets with thinner jet diameter and higher gas density is required for many experimental applications within SPARC. It has been presented in a dedicated technical design report and does not need to be discussed here. The same holds for the development of an electron target which is discussed as an alternative to experiments at the gas-jet target. Due to its favorable geometry, the electron target offers access to X-rays emitted directly by the interaction of the ions with a collinear electron beam under very small observation angles [13].

When the ions interact with the internal targets, they may capture one electron and promptly emit X-rays. These X-rays are detected by the X-ray detectors mounted under a certain angle θ relative to the ion beam. The precision of the line energy in the laboratory frame is determined on the one hand by the energy resolution of the detector, on the other hand by the energy calibration. The better the energy resolution of the detector, the smaller is the number of counts in a line that is needed for a precise determination of the line energy.

To determine the X-ray transition energy in the emitter frame, the experimental values have to be corrected for the Doppler shift according to $E_{em} = E_{lab} \cdot (1 - \beta \cos\theta) \cdot \gamma$ . Therefore, the relative position of the detector with respect to the emitter, namely the interaction zone of ion beam and target, has to be known with high accuracy [13], even if a configuration with θ = 90° is chosen, where the Doppler shift is minimal. In addition, the velocity β of the ion has to be determined with highest precision. Another serious limitation, independent of the intrinsic detector energy resolution, is the so-called "Doppler broadening" of the measured line widths: The finite diameter of the gas jet leads to an emitting sphere with a radius of 1–5 mm. This results in a finite angular distribution, which causes a broadening of the X-ray lines [13], dependent on beam energy and observation angle. It has been demonstrated by the EXL collaboration [14] that it is possible to narrow this angular distribution by using a remotely moveable aperture inside the UHV setup. However, this gain in resolution is paid for with a loss of intensity, which might not be acceptable for experiments with rare or unstable nuclides.

Considering all these effects, it is evident that ion energies as low as possible with a small energy spread of the beam are essential to obtain high accuracy. The combination of ESR with CRYRING will offer these conditions in combination with high beam intensity. When the Doppler broadening becomes negligible, the energy resolution of the applied X-ray detectors will ultimately determine the precision of the measurements.

In contrast, for experiments at the HESR a considerable reduction of the ion energy is not possible. To efficiently excite inner-shell transitions in beryllium-like ions, an initial ion energy of 100 MeV/u or higher is necessary. At the same time, all arguments concerning Doppler corrections apply. To minimize systematic uncertainties, it would be favourable to use the X-ray detectors themselves to determine the Doppler correction factor: The observation of Balmer transitions, which lie at energies around 15–25 keV [6], has already been discussed above. As QED corrections for these transitions are negligible, the precise determination of their transition energy in the laboratory frame provides precise information on the Doppler shift, thus eliminating the systematic errors from the geometrical corrections. However, a precise determination of the transition energies of the Balmer series is much more difficult at high ion energies when they are Doppler-shifted to a transition energy of about 6 keV or even lower. An X-ray detector with an excellent energy resolution of $\Delta E/E \sim 10^{-3}$ at these low X-ray energies as well as a dynamic range large enough to cover low as well as high X-ray energies up to 100 keV is essential to exploit this opportunity. Microcalorimeters offer excellent energy resolution over a large dynamic range and are, therefore, the only option in this case.

## 2.2. Detection principle of microcalorimeters

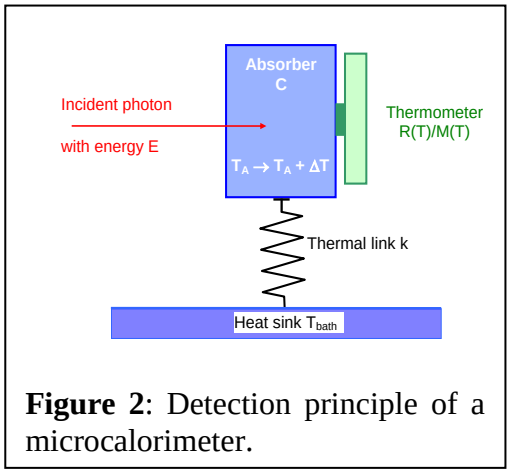


**Figure 2**: Detection principle of a microcalorimeter.

Microcalorimeters detect the temperature change of an absorber after an incoming photon has deposited its kinetic energy as heat. The detection principle is schematically displayed in figure 2: An incoming particle deposits its kinetic energy E in an absorber with heat capacity C, and induces a temperature rise $\Delta T = E/C$. After fast thermalization, the deposited energy is transferred to a heat sink via a thermal coupling k, and the detector returns to its base operation temperature.

To obtain a large temperature signal $\Delta T$, the heat capacity of the absorber has to be as small as possible. Therefore, such detectors are operated at temperatures around 50 mK. Because the generation of phonons – with excitation energies for one phonon of around 1 meV – is almost independent of the absorber material, the absorber can be optimized for a specific experiment with respect to absorber material and size. For X-ray detection, high-Z materials like Pb, Sn or Au are used to combine low heat capacity with high detection efficiency. As the constraints on the heat capacity also limit the active area of one single microcalorimeter pixel to typically 0.5–1 mm², arrays of many detector pixels are mandatory to obtain large solid angles.

To detect the temperature change $\Delta T$, temperature-dependent resistances are the most commonly used thermometer type. A high temperature dependence dR/dT for high sensitivity is achieved either with compensated-doped semiconductors, which have an exponential R(T) characteristic, or superconductors operated at the transition temperature (Transition Edge Sensors, TES). As the phase transition of a superconductor covers only a relatively small temperature range, very high values for dR/dT are obtained, but the dynamic range of a TES is limited. With respect to large arrays, the TES technology offers the additional advantage of an easy multiplexing scheme for many channels. In contrast, the dynamic range of semiconductor thermistors is much larger than the one of TES's. Their dR/dT, however, is one order of magnitude smaller. However, for applications at FAIR, where a large dynamic range is an important requirement,

semiconductor thermistors have been chosen over TES's. Their excellent performance justifies this choice completely.

## 2.3. Detector requirements

To achieve a precision of 1 eV or better for the X-ray transition energy within a reasonable measurement time of one or two weeks, the energy resolution of the X-ray detector has to be below $\Delta E/E \sim 10^{-3}$ for the desired X-ray energies. At the same time, reasonable detection efficiency (including solid angle) of $10^{-5}$ should be obtained. Considering the fact that the energy resolution of a microcalorimeter is determined to a large extent by its heat capacity, the optimal compromise between detector area, absorber thickness, operating temperature and distance of the detector to the interaction zone of beam and target has to be defined.
To obtain a large solid angle, the microcalorimeter should be placed as close to the interaction zone as possible. On the other hand, the microcalorimeters need to be cooled to their operation temperature of about 50 mK, which is only possible in a $^3$He/$^4$He dilution refrigerator. Therefore, the design of this device has to be optimally adapted to the geometry of the targets as well as the space conditions of the surroundings. One particular advantage of microcalorimeters as compared to crystal spectrometers is the – in comparison – small size of the cryostat. The design of the cryostat should allow to place it very close to the interaction zone, even under angles close to 0° or 180°, which are favorable under the consideration of Doppler corrections [13].
For the microcalorimeters themselves, as detailed above, the energy resolution has to be optimized under the consideration that a large absorber volume increases the overall detection efficiency, but it may decrease the energy resolution if the heat capacity gets too large. Thorough investigations on different absorber sizes and materials have to be performed in order to determine the optimal configuration for X-ray energies in the energy range of 50–100 keV for the application at HESR, ESR and CRYRING.

Whereas ESR and CRYRING provide $10^8$ ions/cycle, HITRAP can store a maximum of $10^4$ ions/s or $10^6$ ions every 100 s. Therefore, large detector arrays with large solid angle and high detection efficiency are essential to keep measurement times at a reasonable level. Naturally, it should be possible to adapt any detector array which is designed for the application at the storage rings for the application at HIRTRAP. However, without the application of X-ray lenses [15], which concentrate the produced X-ray photons and increase their intensity by up to a factor of $10^5$, the statistical uncertainties will be considerable, even with large microcalorimeter arrays. As of now, such X-ray lenses work efficiently only up to X-ray energies around 25 keV. Therefore, it is advantageous to deploy a dedicated detector array optimized for X-ray energies below 25 keV. On the other hand, the use of X-ray lenses will focus the X-rays on a small area of 2-5 mm diameter in the focal plane [21]. This fact reduces the demands on the detector solid angle itself.
Another demand on the detectors in a possible setup at HITRAP is the functionality in an environment with high magnetic fields. Therefore, non-superconducting absorbers with low heat capacity and high detection efficiency for high-energy X-rays will be investigated.

In principle, the large dynamic range of silicon microcalorimeters allows the detection of X-rays covering the whole energy range of interest from 1 keV to about 100 keV. However, as is detailed in the next section, investigations with prototype detectors have shown that it is difficult to find a compromise between sufficiently high detection efficiency at high X-ray energies, realized by a sufficiently thick absorber, and a good

energy resolution at low X-ray energies, which eventually is limited by the absorber heat capacity. Accordingly, for the two different energy regimes of 1 keV to about 20 keV on the one hand and 20 keV up to 100 keV on the other hand, two different detector arrays with different absorber thicknesses will be deployed.

## 3. Results of past and present experiments.

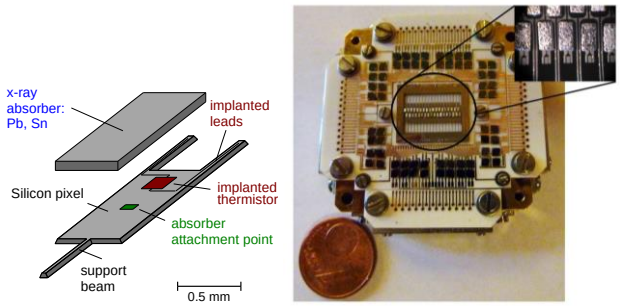


**Figure 3:** A schematic view of a detector pixel for X-ray detection (left side) and a picture of the detector array that has been used for the Lamb Shift experiment on gold. (right side).

The present detector layout is displayed in Figure 3. An array contains two rows with 18 detector pixels each. Each pixel consists of a silicon thermistor, micro-machined from a wafer of silicon and featuring an implanted area (implanted with phosphorus) as the thermometer [16]. Silicon thermistors cover a large dynamic range and are, therefore, best adapted for experiments at storage rings.

As absorber, a thin foil of a superconducting metal with a thickness of around 100 µm is glued onto the thermistor with an epoxy varnish. Due to its high Z value, lead would be the absorber of choice from the point of view of quantum efficiency. However, experiments with a test array have shown that the signal height of lead is reduced as compared to tin for similar heat capacity. Therefore, tin absorbers were chosen for the prototype arrays. Each pixel has an active area of about 0.3 $mm^2$ with a photo peak efficiency of $\geq$ 30% at 100 keV. The detector arrays are glued onto a board of aluminum oxide ceramics (99% $Al_2O_3$). This material ensures a good heat sinking of the detectors by its very good heat conductivity at cryogenic temperatures. In addition, its coefficient of thermal expansion matches the one of copper, thus minimizing mechanical stress of the setup.

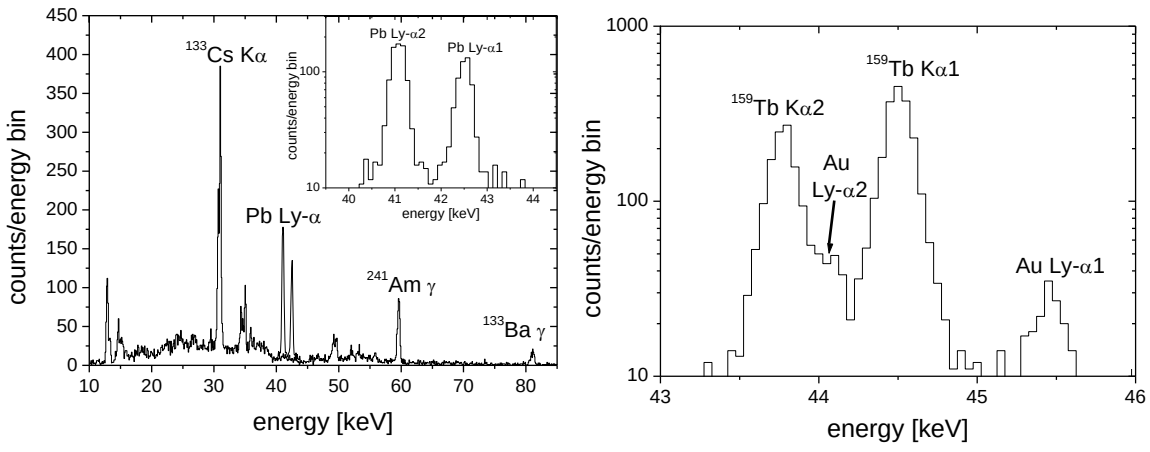


**Figure 4**: Example spectra of the measurement of the Lyman-α transition energies for $^{207}Pb$ (left side) and $^{197}Au$ (right side), including the calibration lines. The displayed spectra are not yet corrected for the Doppler shift [17,18].

At an operating temperature of 50 mK, an excellent energy resolution of the order of $\Delta E \sim 50$ eV for $E_\gamma = 59.5$ keV has been achieved under laboratory conditions for all pixels. Two prototype arrays have been successfully applied in experiments for the determination of the 1s Lamb shift in hydrogen-like ions in the recent past (Figure 4). In these experiments, an energy resolution of down to 75 eV for energies around 60 keV was demonstrated when operated at the ESR. The stability of the operation temperature was monitored using a calibration line of well-defined X-ray energy, which was also used for energy calibration. Slow drifts of the operation temperature with a time scale of several hours were corrected which improved the energy resolution of the X-ray lines [17,18]. For the 1s Lamb Shift of hydrogen-like lead, with a test array of five pixels an energy resolution of $\Delta E/E = 4 \times 10^{-3}$ was obtained. The overall accuracy of the transition energy amounted to ±26 eV [17]. This accuracy was recently improved in an experiment on hydrogen-like gold with a second prototype array of 16 pixels to a value of ±8 eV [18]. The results of these two experiments showed that the accuracy of the Lamb shift determination was not limited by statistical uncertainties or intrinsic detector properties, i.e. energy calibration. In fact, it was limited by the determination of the emission angle θ of the X-rays. Even though the dynamic range of the microcalorimeters is large enough to simultaneously detect also X-rays from the Balmer series, it turned out that the heat capacity of the pixels, which is optimized for energies around 60 keV, limits the energy resolution for X-rays with an energy of around 10 keV, where the Doppler-shifted Balmer X-ray lines are located. Therefore, it was not possible to use the energies of the Balmer lines to independently determine the Doppler correction. As a consequence, the Doppler correction had to be determined by measuring the exact position of the detectors with respect to the gas-jet. This measurement is the main source of uncertainty for these experiments (see [17,18] for a more detailed discussion).

## 4. Technical specification and design details

### 4.1. Next-generation microcalorimeter arrays

As discussed in section 2.3, two detector arrays with different absorber thickness will be prepared. The first detector array will be applied mainly at the ESR and CRYRING as well as the HESR. The major part of the array will be equipped with absorbers optimized for high X-ray energies around 80 keV, namely Sn absorbers. For a thickness of 100 µm, the absorption efficiency ranges from 10% at 100 keV to 100% at 10 keV X-ray energy. These detectors will be similar to the detectors of the two arrays already in operation.

As was discussed in detail in section 2, measuring the transition energy of the low-energy Balmer transitions in hydrogen-like ions simultaneous to the high-energy X-rays is a mandatory task for a next-generation microcalorimeter array. The independent determination of the Doppler correction factor will eliminate the uncertainty from the determination of the emission angle and, therefore, improve the accuracy of the transition energy in the emitter frame. To minimize systematic uncertainties, high resolution and detection efficiency at X-ray energies of 5–15 keV are required in addition to optimal performance at energies around 80 keV. Therefore, a small number of pixels will be equipped with thinner absorbers optimized for X-ray energies below 20 keV, the optimal range for the Doppler-shifted Balmer transitions. For these energies, absorbers of CVD-grown HgTe, as used by NASA for energies below 5 keV [16], will be applied. With a film thickness of 1 µm, the absorption efficiency ranges from almost 100% at 1 keV to around 10% at 10 keV. The NASA/Goddard group has obtained an excellent energy resolution of below 4 eV at 5 keV with such absorbers. Our collaboration will rely on their expertise for the production as well as the attachment and optimization procedure.

This detector array for high X-ray energies will also be applied at HITRAP provided that the X-ray intensity is sufficiently high either by minimizing the distance of the detector to the interaction zone or by using intense liquid-drop or even solid interaction targets. However, as was detailed in section 2.3, a second detector array will be prepared which is optimized for X-ray energies below 20 keV. This second detector array will be equipped entirely with absorbers of CVD-grown HgTe.

Apart from the different absorbers, these two arrays will be identical in design and production. The arrays themselves are provided by our collaborators from the NASA/Goddard Space Flight Center. Each array is glued onto a ceramic board with vapor-deposited leads. The electrical connection between each pixel on the array and its contacts on the ceramic board is provided by ultra-sonic bonding. The Justus-Liebig-University has a laboratory for micro- and nano-structuring (cleanroom class 1000 and 10000) which is equipped with an ultrasonic bonder for this purpose. The absorbers are glued onto the detector pixels after electrical contact has been established and the connection of all pixels has been tested.
As can be seen from the scheme in figure 5, the detectors are operated in parallel with a high-resistivity load resistor in order to minimize electronic noise contributions from the detector bias. These load resistors are glued onto a separate ceramic board and contacted to the detector board via ultra-sonic bonding. This modular design is on the one hand favorable to minimize mechanical stress on the setup during the procedure of cooldown to cryogenic temperatures. On the other hand, it facilitates the repair or exchange of the different components. All ceramic boards are screwed onto a copper holder which is mounted onto the cold finger of the cryostat. Whereas the ceramic boards have to be produced by a specialized company, all copper parts will be manufactured from high-purity copper by the mechanical workshop of the Institute for Atomic and Molecular Physics in Gießen, who have long-standing experience with the production of vacuum and low-temperature pieces.
The most challenging part of this production procedure is to optimally design the

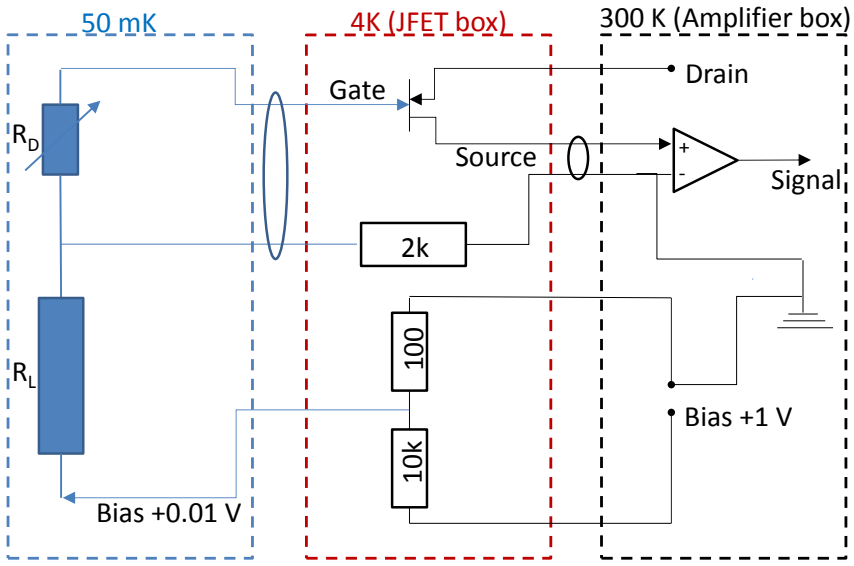


**Figure 5:** Readout scheme for silicon microcalorimeters. $R_D \approx 6\,M\Omega$ denotes the resistance of the microcalorimeter, $R_L = 60\,M\Omega$ is the load resistor. The box with the junction field effect transistors (JFETs) is mounted at 4 K, however the JFETs are operated at 120 K.

array and load resistor boards. For this design, we will rely on the design of the prototype array. However, some improvements have been identified in the prototype arrays which will be included in the next-generation design. These improvements refer in particular to the electrical paths on the load resistor board. As compared to the setup shown in figure 4, the load resistor boards will be mounted at an angle of 90° with respect to the detectors. Figure 6 shows a drawing of the design of the next-generation detector array. The array is mounted in the front of a copper holder which connects the whole setup to the 10 mK stage of the cryostat. The load resistor boards are mounted on the sides and connected with high-density plugs to the detector array. This configuration is more compact than the one used in the prototype array. However, energy resolution and overall performance have to be investigated.

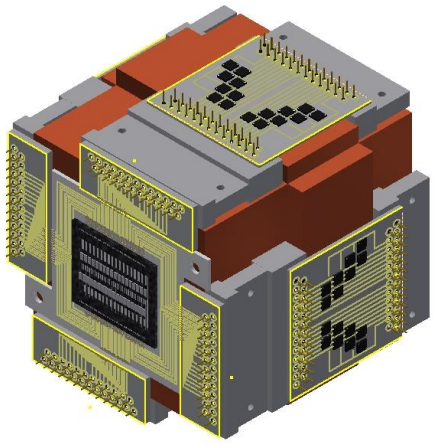

**Figure 6**: Design of the next-generation detector array.

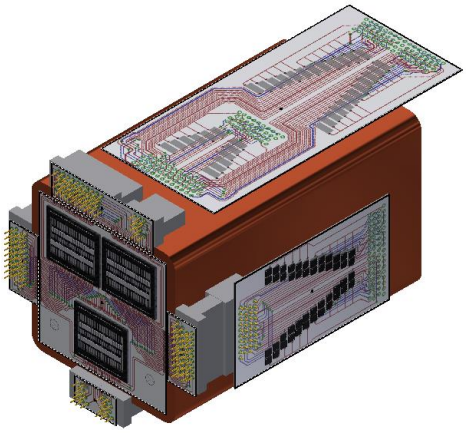

**Figure 7**: Preliminary design study for three arrays

Depending on the expertise gained with these two arrays of 32 pixels, as a next step a triple array with 96 pixels will be equipped. Concerning cooling power and electrical feedthroughs, the cryogenic setup is designed to house up to 100 detector pixels. However, to place three arrays the detector holder as to be redesigned completely. The experiences gained with the new concept of separated detector array board and load resistor boards will be taken into account. For the load resistor boards, an increase from 8 pixels per board as of now to 12 pixels per board, which is mandatory to read out 96 pixels, is straight forward. However, new cables with more leads on the detector front end will be needed. A preliminary design with three arrays is displayed in figure 7.

### 4.2. Readout Electronics and Data Acquisition

The readout electronics and data acquisition are the same for all detector arrays (see figure 5). As a first readout stage, cold junction field effect transistors (JFETs), which are placed inside the cryostat, are used. They serve as impedance matching to match the high impedance of the detectors of several Mega-Ohms to the low impedance of the cables connecting the detectors with the room-temperature electronics. The JFETs, which work at an operating temperature of 120 K, are housed in gold-plated boxes and placed as close to the detector array as possible. Currently, each JFET box is designed to house eight JFETs. Eight boxes are foreseen inside the cryostat, therefore, 64 detector pixels can be readout with the current design without changes. To read out a larger number of detector pixels, a re-design of the JFET board will be necessary. Each box will then house 12 JFETs. As for the detector arrays themselves, a staged approach

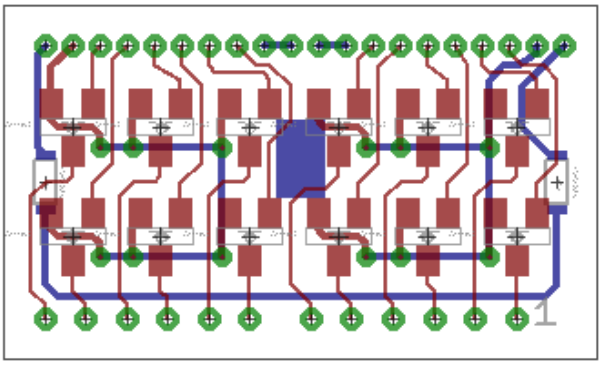

**Figure 8**: Printed circuit board for one JFET box with 12 JFETs. The diode and resistance in the center are used to stabilize the operation temperature to about 120 K. The JFETs will be soldered onto the board rather than bonded, which considerably facilitates the production.

starting with the already tested design and then advancing towards a larger number of JFETs will be taken. As compared to the JFET board used in the past experiments, a new board has been designed with a new JFET type, which can be soldered onto a printed circuit board (PCB, see figure 8), as compared to the type currently in use which has to be bonded. This will facilitate the production of the JFET boards considerably, because the time-consuming bonding procedure will be avoided. Replacing a single JFET on the boards will be easy and fast.

The JFETs are connected to voltage-sensitive preamplifiers at room temperature. These amplifiers are based on amplifiers designed by McCammon et al. [19]. They are especially adapted to the relatively slow signals of the microcalorimeters. One amplifier box is connected to each JFET box and currently houses eight amplifiers as well as the bias supply for the detectors and the JFETs and the JFET temperature regulation. The amplifiers, designed by technicians from Mainz University, consist of printed circuit boards (figure 9), which house four amplifier circuits each. An extension to twelve amplifiers per box will, therefore, be obtained very easily and without major design efforts by simply adapting the main input printed circuit board.
The preamplifier signals are digitized by 24-bit channel-to-channel-isolated ADCs with Anti-Aliasing Filter (National Instruments NI 9239, four channels per module) and a digitization rate of 50 kS/s. The ADC data are transferred to a FPGA Controller (NI PXI 7813R) with 40 MHz frequency and 216 kByte embedded block RAM. To read out 32 channels, two FPGA controllers are used. To allow for flexible signal length, a versatile algorithm will be developed to digitize the signals and determine the trigger level, which means that every channel triggers and is read out independently. All parameters of the signals can be chosen freely up to the maximum digitization rate of 50 kHz, which is more than sufficient to digitize the relatively slow detector signals. The setup will be modular and can, therefore, be extended to a larger number of channels easily. The modules of the company National Instruments provide a reasonable compromise between high performance and relatively low price. Nevertheless, the extension to 96 channels will be the most cost-intensive part of the development work.

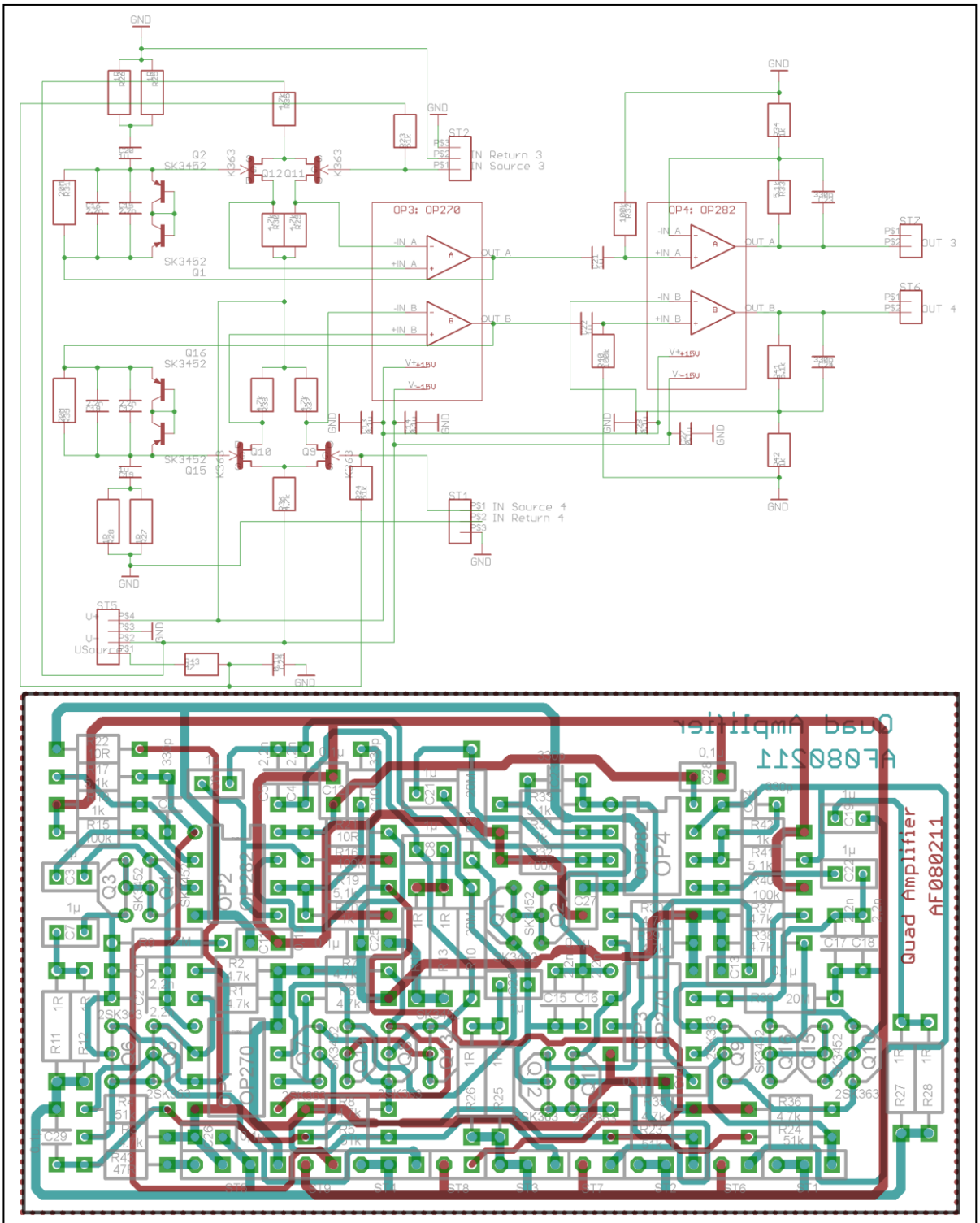


**Figure 9:** Schematic layout and printed circuit board for a board with four amplifier channels (designed by technicians from Mainz University). In the schematic layout, only two channels are shown.

## 4.3. The adapted $^3$He/$^4$He Dilution Refrigerators

To obtain a reasonable solid angle, the detectors have to be located as close as possible to the interaction zone at the internal gas-jet target. Accordingly, a special $^3$He/$^4$He-dilution refrigerator with a side arm which fits to the internal target geometry was designed [9] and commissioned in 1998. A schematic view of the system is displayed in figure 10: The detectors are mounted on the tip of the cold finger and connected via a thick copper rod to the mixing chamber, which stays at a base temperature of 11.5 mK. Bicycle wheels of nylon are used for vibration damping and thermal decoupling of the cold finger from the outer stages, in particular the 4 K stage which houses the JFET boxes. A vacuum vessel as well as three shields at 77 K, 4 K and 900 mK shield the detectors against thermal radiation from room temperature. The X-rays pass a system of four aluminum-coated mylar windows in front of the detectors. The thin aluminum coating allows for an overall transition efficiency of ≥ 90% for X-ray energies at 1 keV and more than 99% for X-rays at 100 keV while maintaining an operating temperature of the detectors of about 50 mK. In order to suppress low-frequency microphonic noise, the JFET boxes have to be placed as close as possible to the detectors without introducing too much thermal radiation. At the same time, the outer diameter of the cold finger is limited by the experimental conditions at the ESR, namely the inner diameter of a standard CF-100 flange, to approximately 90 mm. Therefore, the cold finger consists of a thicker part which houses the JFET boxes, and a thinner part which is placed inside a vacuum pocket at the gas-jet target. However, producing new shields with different geometry poses no particular difficulty if experimental conditions demand it.

The cryostat – denoted as "wet system" in the following discussion – uses liquid nitrogen and liquid helium as consumable cryogenics; repeated refills of cryogenics are, therefore, unavoidable during beam times. The consumption of liquid helium amounts to about 100 l per week. To avoid this costly and time-consuming disadvantage, a new $^3$He/$^4$He-dilution refrigerator with similar design, which runs without the supply of cryogenic liquids ("dry system") and is adapted to fit the geometry of the internal gas-jet target at the ESR as well as at the HITRAP facility [20], is currently under commissioning. As compared to the wet system, this new cryostat is smaller, lighter and more versatile in design. These features will allow to place it not only at the foreseen gas-jet targets, for which a dedicated mount is readily available from the former ESR experiments. Due to its low weight, it can also be placed above a beamline, e.g. at the foreseen electron targets. Mounting the cold finger

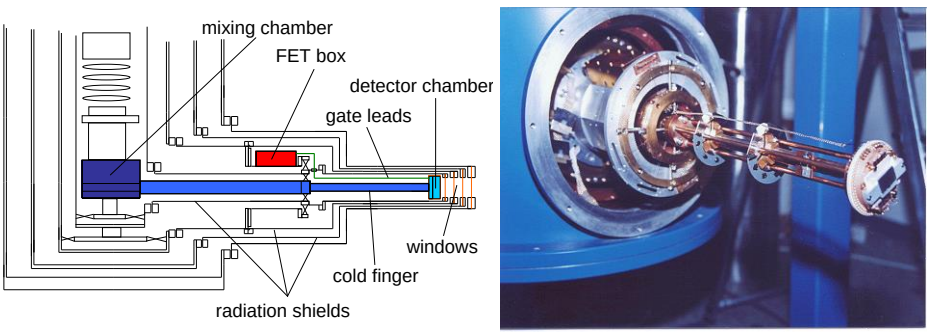


**Figure 10:** Schematic view (left side) and picture (right side) of the side arm of the $^3$He/$^4$He dilution refrigerator which houses the silicon microcalorimeters (wet system) [9]. The microcalorimeter array is mounted on the tip of the cold finger. In the left upper corner, one of the gold-plated JFET boxes is visible.

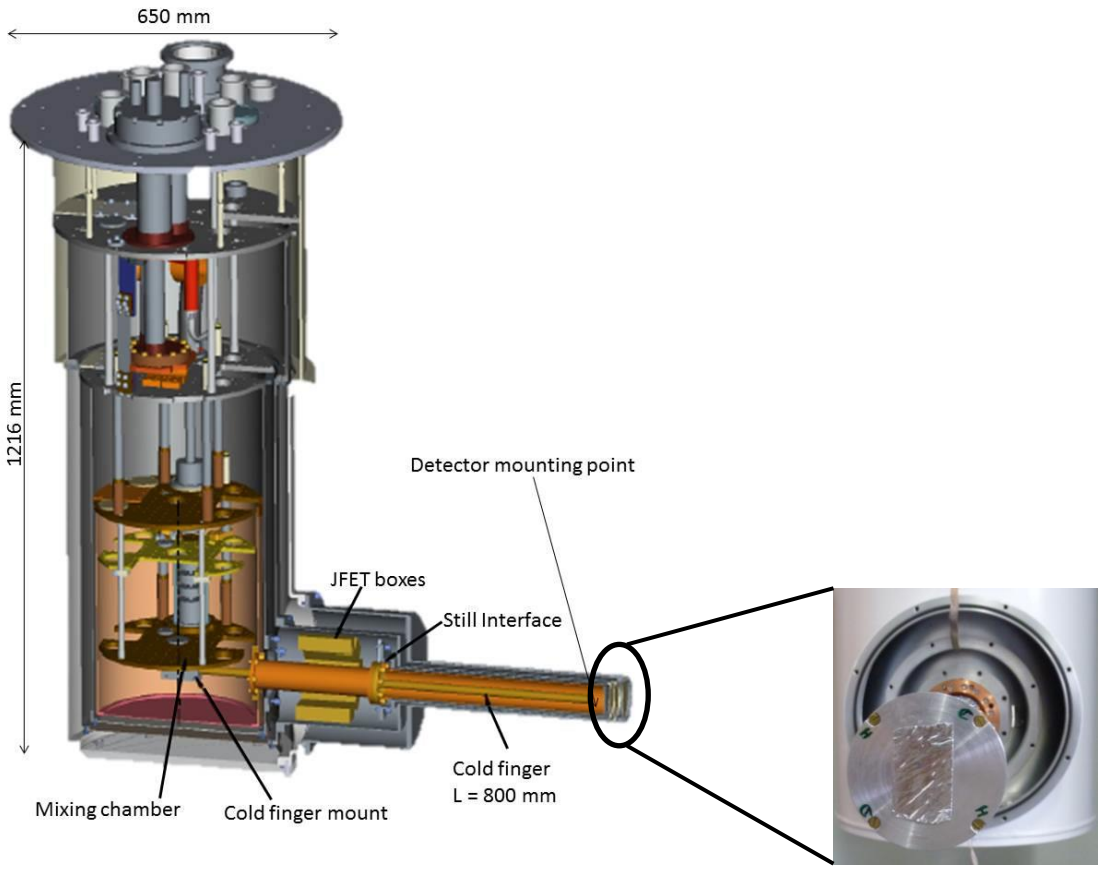


**Figure 11:** Schematic view (left side) and picture (right side) of the cryogen-free $^{3}He/^{4}He$ dilution refrigerator (dry system) [20]. The microcalorimeter array is mounted on the cold finger. As compared to the wet system in figure 10, a more versatile design is realized.

in a perpendicular position below the system is a possibility that can be realized by simply changing the design of the shields and producing an adequate vacuum interface. This option is not available with the wet system, where the whole inner vacuum vessel is immersed in liquid helium and not accessible from below. However, it has to be stated that both systems can be operated in parallel if supply of cryogenic liquids is available. As both cryostats are foreseen to house 96 detector pixels each, this would then amount to a total of 192 detector pixels, with the possibility to place two detector arrays also under different observation angles. In combination with future magnetic microcalorimeters, a setup of several microcalorimeter arrays will be possible which will offer not only enhanced detection efficiency, but also the option of determining angular distribution of X-rays, which may be interesting for quite a few experimental investigations.

## 5. Radiation environment, safety issue

The wet cryostat uses liquid nitrogen and liquid helium as cryogenic liquids. An according ventilation of the experimental site is necessary.

## 6. Production, Quality Assurance and Acceptance Tests

The development of the new detector arrays as well as first stages of commissioning will be performed in the laboratories of the universities in Gießen and Mainz with standard X-ray calibration sources. Once the detector arrays are working with optimal performance, commissioning at the ESR or CRYRING will be mandatory.

## 7. Calibration with test beams

Several short commissioning beam times would be preferable to investigate the experimental conditions at the storage rings and consider any potential negative influences of the surroundings. Experience from prior experiments at the ESR has shown that it is necessary to optimize the experiment electronics, cables and potentially electromagnetic shielding in the case of high magnetic fields as may occur when applying such detectors at HITRAP. These commissioning beamtimes will need heavy, highly charged ions like hydrogen-like lead or gold at low ion energies. The operation of a gas-jet target will be required to produce X-rays. For commissioning, experiments at an electron target would be less favorable, because so far no experience exists with such a setup.

## 8. Civil engineering, cave, cooling, cranes etc.

The cryostats will be mounted on a special mount which has been designed to fit the limited space at the ESR gas-jet target. It needs an area of about 1 m². The $^{3}$He/$^{4}$He circulation system is operated with three-phase power and requires no extra cooling. It should be placed close to the cryostat and requires a space of approximately 2 m².
The wet system has a height of 200 cm. There above, a space of approximately 150 cm is required for refilling the cryogenics. The empty cryostat weighs about 100 kg. Some type of lifting equipment is needed to place it on its mount before an experiment. After filling, the system should not be moved.
The dry system has a height of 150 cm and weighs about 70 kg. It does not need any cryogenic supply from outside except a small amount of liquid nitrogen for an external cold trap. For the latter, the consumption does not exceed 20 l per week and is, therefore, comparable to the liquid nitrogen consumption of a standard germanium detector. As the valves of the $^{3}$He/$^{4}$He operating system are operated with pressurized air, an according supply at 5 bar has to be provided. The pulse tube cooler runs with three-phase power and is water-cooled. It has a power consumption of about 12 kW. Therefore, it needs a flow of minimum 9 liters per minute dependent on the temperature of the incoming water. The $^{3}$He/$^{4}$He circulation system is operated with standard two-phase power and does not need any additional cooling. As all infra-structure is included in a wheeled rack, it does not need more than 1 m² of floor space. Its weight amounts to about 300 kg. The cryostat can be mounted on a mount similar to the one used for the wet system or onto any mount adapted to experimental needs. As the amount of cryogenic liquids is very small and operated in a closed cycling system, requirements on the mount stability do not exceed standard safety considerations. A small electronic rack is used to operate the cryostat. This rack does not need to stay as close to the cryostat as the $^{3}$He/$^{4}$He operating system. A distance of up to 5 m is acceptable. In addition, the system can also be operated via USB or Internet connection from any computer outside of restricted areas.

## 9. Installation procedure, its time sequence, necessary logistics from A to Z including transportation

As the silicon microcalorimeter array has already been applied at the internal gas-jet target at the ESR, the setup is well tested. It can be moved to a new experimental site without major modifications. The cryostat that contains the microcalorimeters can be placed at any position which offers a CF100 or larger viewport and a thin vacuum window. No direct connection between the vacuum of the storage rings and the vacuum of the cryostat is intended.
Figure 10 shows two pictures of the two cryostats, namely the wet system installed at the ESR and the dry system in the laboratory. As for requirements on infrastructure, the wet system requires a constant supply of liquid helium and liquid nitrogen, about 100 l per week for both cryogenics. A recirculation of the liquid helium would minimize the costs if it is readily available, but it is no necessary prerequisite for the operation.

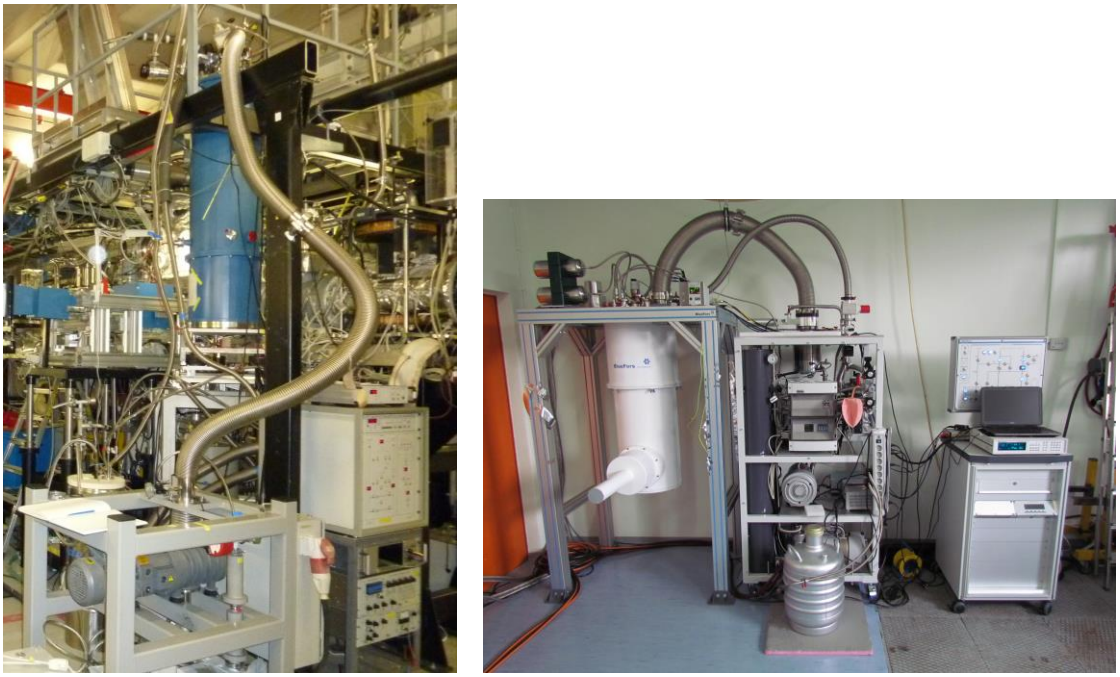

**Figure 12:** Examples for the installation of silicon microcalorimeters:
Left side: The wet system installed at the ESR for the Lamb shift experiment.
Right side: The new, dry system installed in the laboratory at the Justus-Liebig-University Gießen.

## 10. References


[1] SPARC Technical Proposal (2006), 41
https://www.gsi.de/start/fair/fair_experimente_und_kollaborationen/sparc/dokumente.htm
[2] Th. Stöhlker et al., Lecture Notes in Physics **745** (2008) 157
[3] S. Fritzsche et al., J. Phys. B: At. Mol. Opt. Phys. **38** (2005) S707
[4] C. Z. Dong et al., Journal of Physics B **39** (2006) 3121
[5] S. Trotsenko et al., J. Phys. Conf. Ser. **58** (2007) 141
[6] R. Reuschl et al., Radiation Physics and Chemistry **75** (2006) 1740
[7] P. Egelhof et al., Nuclear Instruments and Methods A **370** (1996) 263
[8] P. Egelhof and S. Kraft-Bermuth, Topics in Applied Physics **99** (2005) 469
[9] A. Bleile et al., AIP Conference Proceedings **605** (2002) 409

[10] H. Beyer et al., Spectrochimica Acta B **59** (2004) 1535
[11] A. Fleischmann et al., Topics in Applied Physics **99** (2005) 151
[12] C. Pies et al., J. Low Temp. Phys. **167** (2012) 269
[13] A. Gumberidze et al., Physical Review Letters **94** (2005) 223001
[14] M. von Schmid et al., GSI Scientific Report (2012) 207
[15] S. G. Podorov et al., Journal of Physics D **34** (2001) 2363
[16] C. Stahle et al., Nuclear Instruments and Methods A **310** (1996) 173
[17] V. A. Andrianov et al., Journal of Low Temperature Physics **151** (2008) 1049
[18] S. Kraft-Bermuth et al., Journal of Low Temperature Physics **176** (2014) 1002
[19] M. Weber, Diploma Thesis, Johannes-Gutenberg-Universität, Mainz (1998)
[20] S. Kraft-Bermuth et al., Journal of Low Temperature Physics **167** (2012) 765
[21] B. Grabinger, Master Thesis, Friedrich-Schiller-Universität Jena (2015)